Time-frequency and Time-Scale analysis of Barkhausen noise signals.

Linilson Padovese, Nadine Martin, Fabien Millioz

Time-frequency and Time-Scale analysis of Barkhausen noise signals

Linilson R. PADOVESE
Department of Mechanical Engineering, School of Engineering,
University of Sao Paulo
Av. Prof. Mello Moraes, 2231
Sao Paulo/SP, 05508-900, Brazil
55 11 3091 5590
55 11 3813 1886
lrpadove@usp.br

Nadine MARTIN et Fabien MILLIOZ
GIPSA-lab, INPG/CNRS
Department Images Signal
Grenoble Campus
BP 46 - 961, rue de la Houille Blanche
F-38402 Saint Martin d'Hères – France
nadine.martin@gipsa-lab.inpg.fr
fabien.millioz@gipsa-lab.inpg.fr

Abstract

Carrying out information about the microstructure and stress behaviour of ferromagnetic steels, Magnetic Barkhausen Noise (MBN) has been used as a basis for effective Non Destructive Testing methods, opening new areas in industrial applications. One of the factors that determines the quality and reliability of the MBN analysis is the way information is extracted from the signal. Commonly, simple scalar parameters are used to characterize the information content, such as amplitude maxima and signal root mean square. This paper presents a new approach based on the time-frequency analysis. The experimental test case relates the use of MBN signals to characterize hardness gradients in a AISI4140 steel. To that purpose are assessed different time-frequency and time scale representations such as the spectrogram, the Wigner-Ville distribution, the Capongram, the ARgram obtained from an AutoRegressive model, the scalogram, and the Mellingram obtained from a Mellin transform. It is shown that, due to non-stationary characteristics of the MBN, time-

frequency representations can provide a rich and new panorama of these signals. Extraction techniques of some time-frequency parameters are used to allow a diagnostic process. Comparison with results obtained by the classical method highlights the improvement on the diagnosis provided by the method proposed.

1. Introduction

The Magnetic Barkhausen Noise (MBN) is a magnetic phenomenon produced when a variable magnetic field induces magnetic domain wall movements in ferromagnetic materials. These movements, not continuous but discrete, are caused by defects in the material microstructure, and generate magnetic pulses that can be measured by a coil placed on the material surface. Since the MBN is sensitive to the state of the material microstructure, to the presence of deformations and mechanical stresses, it can be (and has been) used in the development of Non-Destructive Essays regarding several industrial applications [7,10]. Success in the development of inspection systems based on the MBN depends on the synergetic use of knowledge from different areas such as material sciences, electronics, mechanics, and signal processing.

A point, put in evidence by MBN studies, is the importance of a deeper study of signal processing methods allowing better highlighting and separation of MBN signal information concerning the various material states.

The traditional MBN signal processing analysis methods can be classified in two classes: the scalar methods (or 0 dimension methods – 0D) and the vector methods (or 1 dimension methods – 1D). The 0D methods use parameters extracted from the MBN signal, such as Root Mean Square (RMS), energy, maximum value, number of MBN peaks at certain values, or else from the frequency domain, such as the energy at some frequency bands. The 1D class uses the envelope of the time

signal or that of the spectral MBN signal. As one increases the dimension of the analysis methods, the quality and quantity of available information carried out by the signal increase.

However, due to the nature of the Barkhausen signal, e.g., a sequence of discrete magnetic pulses whose physical model is sometimes associated to avalanches belonging to the class of critically self-organized phenomena [6], it seems that other methods of signal analysis would be more adequate as, for example, time-scale methods permitting multiple time-frequency scale analysis, instead of linear analysis characterizing the time-frequency methods commonly used in non-stationary phenomena. Very few works have been published on these subjects, concerning Magnetic Nondestructive methods [3,4].

By analyzing the signal envelope and the spectrum, it is observed that the signal is time limited and wide banded. On the other hand, several questions remain unanswered by this one dimension analysis. For instance: how is the time-frequency structure of MBN? Is there any time-frequency structure that is related with the evolution of stress or with some microstructure variation in the material? Is there any time-scale structure? Is there some informational gain in relation to the traditional scalar and 1D methods? What are the most adequate method of time-frequency (TFR) and time-scale (TSR) representations available in the international literature that best describes the informational content of the MBN signal?

In this context, this work presents the traditional methods of MBN signal analysis, and studies the use of some time-frequency and time-scale representations in the analysis of MBN signals, measured in a 4140 steel that presents hardness gradient.

Moorthy and al. [11] showed that the MBN can be used in order to determine hardness profile of steel specimens. They observed that the MBN level increases with the decrease of hardness, since that the magnetic domain walls can move easier in this case.

Additionally Jeong and al. [10], working with AS 508-3 pressure vase steel, showed that the MBN magnitude varies inversely with hardness, since high values of hardness are related with the increase of discordance density, which are barriers to the wall domain movement. In another work, Moorty and al [12] studied the hardness variation in a weld joint, obtaining results similar to those of present in [11].

It is important to note that the experimental evidence of hardness increase with decrease of MBN activity is general, and sometimes not clearly perceptible by the use of traditional MBN parameters. This paper shows that the use of TFR and TFS can improve informational description of MBN signals.

Section 2 presents the experimental measurements methodology. Section 3 and 4 sum up the time-frequency and time-scale methods considered. Section 5 comments the differences between the representations obtained. Section 6 presents the results of the study. In Section 7, some results obtained by using extraction characteristics techniques from the time-frequency domain are presented.

2. Experimental Measurements

The hardness gradient was produced by Jominy essay in a SAE 4140 steel cylinder. This alloyed steel has a relatively high hardening ability and high strength, and is among the most widely used versatile machinery steels (such as shafts, gears, bolts, couplings, spindles …).

After this, the cylinder was cut longitudinally in two equal parts, and measurements of Rockwell C hardness and MBN signals were made, in the centre line of the flat surface, in points starting 0.3” from the edge until 1.3”, spaced by 0.2” (6 points), as illustrated in Figure 1.

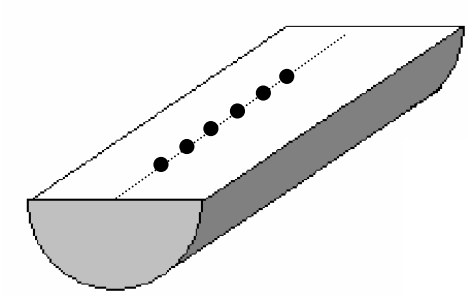

Figure 1. Measurements points to determine the Jominy hardness profile.

The measurement arrangement is schematically shown in Figure 2. A Personal Computer with a data acquisition device (with A/D, D/A and D/D channels) supplies a sinusoidal wave of 10 Hz, which is amplified by a bipolar source that feeds the magnetic circuit in order to magnetize the sample with a magnetic field, producing magnetic saturation in the samples. The MBN sensor output is amplified and band pass filtered (1 - 100 kHz) and digitalized with a sampling frequency of 200 kHz. Each registered signal has the magnetic response of 2 cycles of magnetic excitation.

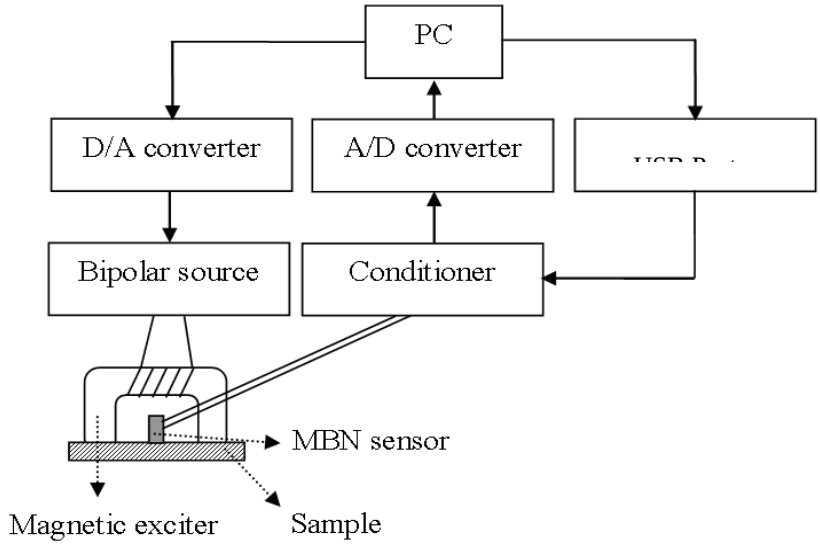

Figure 2. Experimental setup for MBN signal measurements.

3. Time-Frequency Representations

The signal processing methods used are well known in the literature. So the aim of this section and the next one consist only to give a quick overview and a suitable entry point for further reading.

Time-frequency representations are characterized by a fixed resolution in the entire time-frequency domain. Four of them have been considered:

- the spectrogram, the more classical and the more robust;
- the Wigner-Ville distribution and its smoothed version, which belong to the same class than the spectrogram, the Cohen class, and well known for its higher resolution and the presence of interference;
- the Capongram, middle representation between those of the class of Cohen and the parametric representation, interesting for good statistical properties at the expense of computing time;
- the ARgram, a parametric approach.

The latter two have been adapted to nonstationary signals by a simple gliding time window.

3.1 Spectrogram

A linear TFR based on the Fourier transform can be reached by pre-windowing the signal around a chosen time, calculating its Fourier Transform, and proceeding in the same way for each instant. This transform is known as Short Time–Fourier Transform and referred to as *STFT(t,f)* where *t* is the time variable and *f* the frequency variable. A quadratic form related with the Short Time–Fourier Transform can be obtained by taking the square of this transform. It is known as

spectrogram and measures the spectral energy density of the signal in the time–frequency domain. The spectrogram of a signal *x(t)* is referred to as *SPECT(t,f).* The following holds

$$SPEC(\mathrm{t,f}) = \left| STFT(\mathrm{t,f}) \right|^2 = \left| \int_{-\infty}^{\infty} x(\tau) h^*(\tau - t) e^{-j\,2\pi f\,\tau} d\tau \right|^2 , \qquad (1)$$

where *h(t)* is a sliding weighting window and the superscript * denotes conjugate.

The time resolution of the spectrogram is determined by the length of the selected sliding window *h(t),* and the frequency resolution is defined as the –3 dB bandwidth of the spectral window, the spectral window being the spectrogram of the window *h(t).* The best frequency resolution is achieved with the natural window and defined as $\Delta f = 1/D$, where *D* is the time duration of the window. Any other different window will degrade the resolution but improve the estimation variance. The product $\Delta f \times D \geq 1$ measures the joint time-frequency resolution of the method. This resolution limitation is the most significant drawback of the spectrogram. Other major problems can be cited: (a) the implicit windowing problem that causes the “leakage” phenomenon, and (b) the impossibility of averaging periodograms for reducing the estimation variance when working with short data. Nevertheless one advantage of this method is its robustness towards the nature of the signal. See [14] for further reading.

3.2 WV and SPWV

The Cohen class is a general formulation for non-parametric time-frequency distribution, which includes the Wigner-Ville Distribution and relatives. The spectrogram can be considered as a special case of the Cohen class. The Wigner-Ville Distribution of a signal *x(t)* is referred to as *WVD(t,f)* and can be defined as

$$WVD(\mathrm{t,f}) = \int_{-\infty}^{\infty} x(t + \tau/2) x^*(t - \tau/2) e^{-j\,2\pi f\,\tau} d\tau \,. \qquad (2)$$

Since the value of the *WVD(t,f)* is determined by all the values of the signal (and therefore, not limited by a time window), the Wigner-Ville Distribution overcomes the spectrogram trade-off between time and frequency resolution, the hypothesis of short-term stationarity is no more necessary. This improvement comes at a price of the appearance of spectral cross-terms, which comes from the bilinear kernel of the transform. This spectral interference is critical in multicomponent signals, since it makes difficult the distinction of weaker signal components and it masks spectral features.

To overcome this major drawback, several modifications have been proposed and can be found in the literature. One of them, the Smooth Pseudo Wigner Ville Distribution is of particular interest to this work since it will be used later to analyse experimental results. The Smooth Pseudo Wigner Ville Distribution of a signal *x(t)* referred to as *SPWV(t,f)* can be defined as

$$SPWVD(\mathrm{t,f}) = \int_{-\infty}^{\infty} h(\tau) \int_{-\infty}^{\infty} g(t-\eta)\, x(\eta+\tau/2)\, x^{*}(\eta-\tau/2)\, d\eta\, e^{-j\,2\pi f\,\tau} d\tau\,, \qquad (3)$$

where *g(t)* is the time smoothing window and *h(t)* the frequency smoothing window. With the introduction of these two windows it is possible to attenuate and to smooth the interference terms of the Wigner-Ville distribution, by independently choosing the type of window and its length. See also [14] for further reading.

3.3 Capongram

The Capon Method or Minimum Variance Method is a nonparametric spectral power estimator having higher frequency resolution than the Fourier Transform based methods. The quantity estimated, homogeneous to the power of signal *x(t)*, is referred to as $P_{CAP}(t,f)$ and is defined by

$$P_{CAP}(t,f) = \frac{1}{\mathbf{e}_p^{H}(f)\, \mathbf{R}_p^{-1}(t)\, \mathbf{e}_p(f)}\,, \qquad (4)$$

where $e_p^T = \left(1, e^{-2\pi i f\, ts}, \ldots e^{-2\pi i f\, p\, ts} \right)$, *ts* is the sample interval, the superscripts *H* denotes conjugate transpose, *p* is the order of the Capon filter. $R_p(t)$ is the correlation matrix of dimension $(p+1)\times(p+1)$ evaluated on a gliding time window centred at the time instant *t*.

The signal power obtained by this approach can be seen as the output of a filter, of length *p* and with variable center frequency. Parameter *p* has to be chosen by the user and plays a leading role in the performance level.

The design of the Capon method allows the frequency resolution to be high on a short time window. This approach assumes signal stationarity over the time window and, therefore, is appropriated to analyze weakly non-stationary signals. See [15] for further reading.

3.4 Argram

The gliding power spectrum density of the Autoregressive Model of a signal $x(n)$, referred to as $S_{AR}(t,f)$, can be obtained by

$$S_{AR}(t, f) = \frac{P_w}{\left| 1 + \sum_{k=1}^{p} a_{k,t}\ e^{-j2\pi f\, k} \right|^2} \quad , \qquad (5)$$

where P_w is the power of the white noise (or the prediction error), *p* is the model order and $a_{k,t}$, the model coefficients evaluated on a time gliding window centred at time *t*. This equation is also known as the Maximum Entropy Spectrum. The choice of the order *p* is done by the user and constitutes the main issue of this approach. This order is related to the number of components of the signal.

As for the Capon method, the AR model allows the frequency resolution to be high on a short time window. This approach assumes signal stationarity over the time window and, therefore, is appropriated to analyze weakly non-stationary signals. See [16] for further reading.

4. Time-Scale Representation

Time-scale representations are characterized by a variable resolution in the time-frequency domain, where the frequency is the inverse of the scale unit. Two time-scale transform have been considered:

- a scalogram as a classical time-scale transform;
- a Mellingram as an adaptation of the Mellin transform for nonstationary signals.

Scalogram

The Scalogram is a time-scale representation based on the Wavelet Transform, referred to as $Tx(t,a;\Psi)$ and defined by

$$Tx(t,a;\Psi) = \int_{-\infty}^{\infty} x(s)\Psi_{t,a}(s)ds\,, \qquad (6)$$

where $\Psi_{t,a}(s) = |a|^{-1/2}\,\Psi\left(\frac{s-t}{a}\right)$, and Ψ is the mother wavelet. Parameter *a* is the scale factor. Although the representation obtained is time-scale, it is possible to establish an associated time-frequency representation, by using the relation $f = f_0 / a$, where f_0 is a reference frequency of the mother wavelet. See [19] for further reading.

4.2 Mellingram

Several transforms have been proposed in order to operate a space transformation, with the objective of facilitating interpretation of a physical phenomenon. One of these transforms is the Mellin Transform. The gliding Mellin transform of a signal x(t) referred to a $M_x(t\,;\,p)$, can be deduced from its general form [1, 2] and is given by

$$M_x(t\,;\,p) = \int_0^{\infty} x(\tau)\,w(t-\tau)\,t^{p-1}d\tau\,, \qquad (7)$$

where *p*, a complex number, is the Mellin parameter and w(t) a time window.

A particular form of the Mellin transform, also named Scale Transform, is obtained by using *p=-jc+1/2*, with c a real number. Therefore, adapted to nonstationary signals, a gliding Scale transform, referred to as $D_x(t\,;c)$, is

$$D_x(t\,;c)=\frac{1}{\sqrt{2\pi}}\int_0^{\infty} x(\tau)\,w(t-\tau)\,e^{(-jc-1/2)\ln\tau}\,d\tau\,. \qquad (8)$$

If *x(t)* is a function and *g(t)* is a scaled version of *x(t)*, then the amplitude of the transform will be the same. If *x(t)* has a scale periodicity of period τ, then $x(t)=\sqrt{\tau}\,x(\tau t)$. See [1, 2] for further reading.

5. Vantages and disadvantages of each method

Table 1 presents the values of the parameters used in each method to calculate the TFRs and TSRs, and the computational time consumption for each case.

The Spectogram in Eq. (1) is fast and very easy to use, since the transform does not depend on some *a priori* information (order parameter) as in Argram and Capongram cases. But the estimation has the highest variance and the lowest time-frequency resolution.

The Wigner-Ville distribution in Eq. (2) presents two major advantages: it is a non-parametric method and it has a good time-frequency resolution. Its major drawback is the appearance of spectral cross-terms, which makes difficult the distinction of weaker signal components. Additionally, it masks spectral features.

The Smoothed Pseudo Wigner-Ville distribution defined in Eq. (3) attenuates and smoothes the interference terms, at a cost of some degradation in time-frequency resolution. However, these two methods have a severe limitation related with the computational memory consumption. A PC with a 2-core processor at 3 GHz and with 2GB RAM, as used for the other transform calculation, was not

enough for the Wigner-Ville distribution and Smoothed Pseudo Wigner-Ville distribution, given the length of the recorded signals. In order to get results, a dual 4-core processors at 3GHz and, above all, with 16 GB RAM as specified in Table 1 had to be used. One solution could be to reduce the time signal length. But, the total time duration is given by the materials magnetic behavior and the frequency of the magnetic excitation, which is dictated by the nature of the mechanical or microstructure problem. Furthermore, MBN signals can have a frequency band varying from 100 to 300 KHz. This implies more restrictive constraints than for vibration or acoustic signal analysis, where the frequency band is around 10 or 20 KHz. The PC with 2GB RAM was able to compute the Wigner-Ville transform on 2 500 points only, instead of the 10 000 points. In addition, processing a shorter length should need time segmentation; that is to say a supplementary algorithm to tune in the context of an automatic procedure, which is the final aim of our study. Other solutions consist of using special architecture for running the Wigner-Ville transform; see one possibility in [20].

The Capongram in Eq. (4) has a higher time-frequency resolution and lower variance than the Spectogram, but is more computationally time consuming than this last one and the Argram method (see Table 1). Although the Capongram does not impose a model in the signal, it is necessary to estimate a parameter, named “order” *p* that has a meaning different from the order of the Argram. Meanwhile the AR model order is related with the degree of freedom of the system being modelled, the Capongram order describes the filter length. In the AR model, the order is optimal when its value is close to the system degree of freedom, whereas an increase in the Capon filter bank order increases the frequency resolution at the expense of deterioration of statistical stability.

In other words, in the Argram method the spectral information is contained inside the AR filter and, conversely, is in the output of the filter in the Capongram method.

Table 1. Parameters used in the TFR and TSR calculations-The 16GB RAM was necessary for the Wigner-Ville transform only. For the others a machine with 1GB RAM is enough.

TFR or TSR	***Transform Parameter*** *10 000-point signal length*	***Calculation time relatively to the spectrogram*** with two 4-core processors at 3GHz *with 16 GB RAM*
TFR: Spectrogram	*256 point-Hanning window* *50% overlap* *512 FFT bins*	*1 (reference)*
TFR: Smooth Pseudo Wigner-Ville	*513-point Hanning time window* *2049-point Kaiser frequency window*	*8 349*
TFR: Capongram	*512-point Boxcar window* *25% overlap* *Order-100 Capon filter* *91-frequency bins from bin 5 with step 1*	*308*
TFR: Argram	*512-point Boxcar window 25% overlap* *Order-40 AR filter*	*29*
TSR: Scalogram	*Morlet wavelet* *50 scales*	*471*
TSR: Mellingram	*512-point Boxcar window* *25% overlap*	*26*

The Argram in Eq. (5) is a time–frequency method more adequate to describe narrow band spectral components. The main drawback of this method is, maybe, that it implies an *a priori* knowledge (or assumption) about the process from which the signal is taken. This *a priori* information is expressed by the selection of the model order *p*. A good choice of this parameter is essential for good spectral estimation, what implies an additional computational time in order to find a good value (see Table 1). Other disadvantage is the high computing time necessary to calculate the spectrum in each time moving window (see Table 1). The main advantage of the Argram method is its high time and frequency resolution and its low variance.

Although very time consuming, the highest among the used methods, the Scalogram in Eq. **Erreur ! Source du renvoi introuvable.** is simple to use, depending only on the choice of the

number of analysis scales. Both, the Scalogram and the Mellingram in Eq. **Erreur ! Source du renvoi introuvable.**, are methods that can show scale structures in the signal, if they exist and in a different manner, not identifiable with the traditional time-frequency representations.

6. Results

In what follows, some results of experimental database analysis are shown in a sequence of increasing richness of information representation and, by consequence, also of increasing complexity of analysis and interpretation.

Figure 3 shows the 6 MBN signals, for a measured position, plotted in the same scale, for amplitude comparison. It is possible to notice that the MBN signal changes with the change of hardness. The aim of the signal processing process is to put in evidence if there is some information in the MBN signals correlated with hardness values.

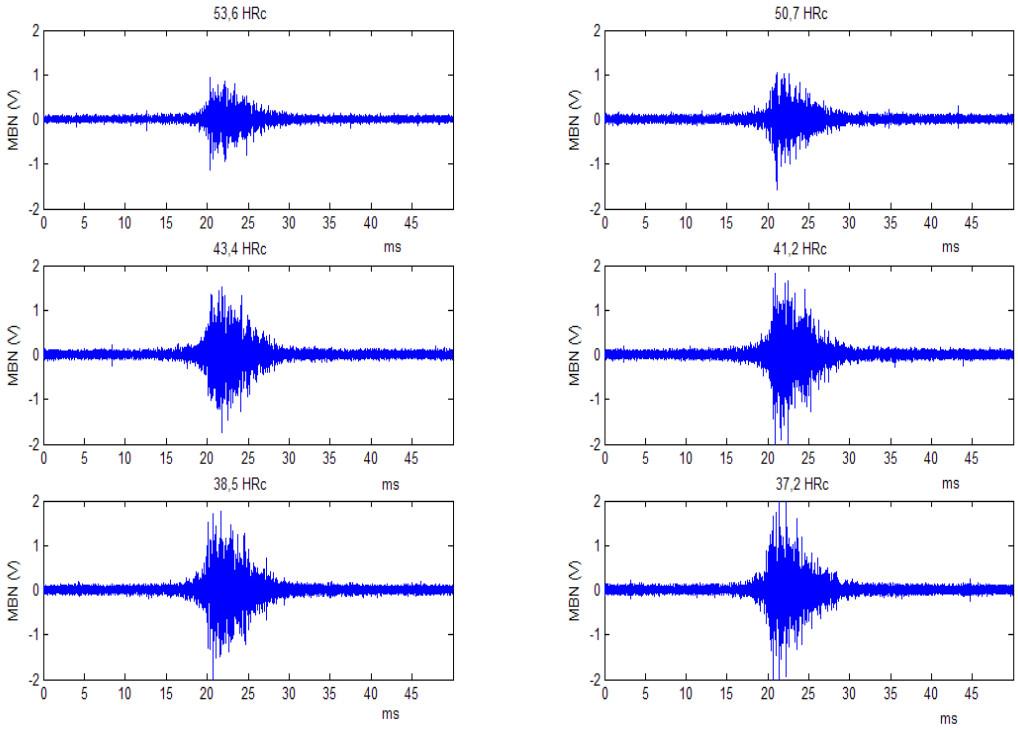

Figure 3. MBN signals measured with the experimental setup for different hardnesses in a AISI4140 steel.

Figure 4 shows the hardness and the average of 6 MBN RMS values, measured throughout the sample at the 6 already mentioned positions. These results agree with what is reported in the international literature since, globally, the MBN RMS values increase with the decrease of hardness. Nevertheless, the last value of the MBN RMS does not agree with this tendency. In this context, one should ask if it is the correlation hardness x MBN that failed or it is this parameter, RMS, which cannot correctly describe the correlation. It is well known that the simpler the parameter used to describe the informational countenance of a signal, the poorer the information it gives.

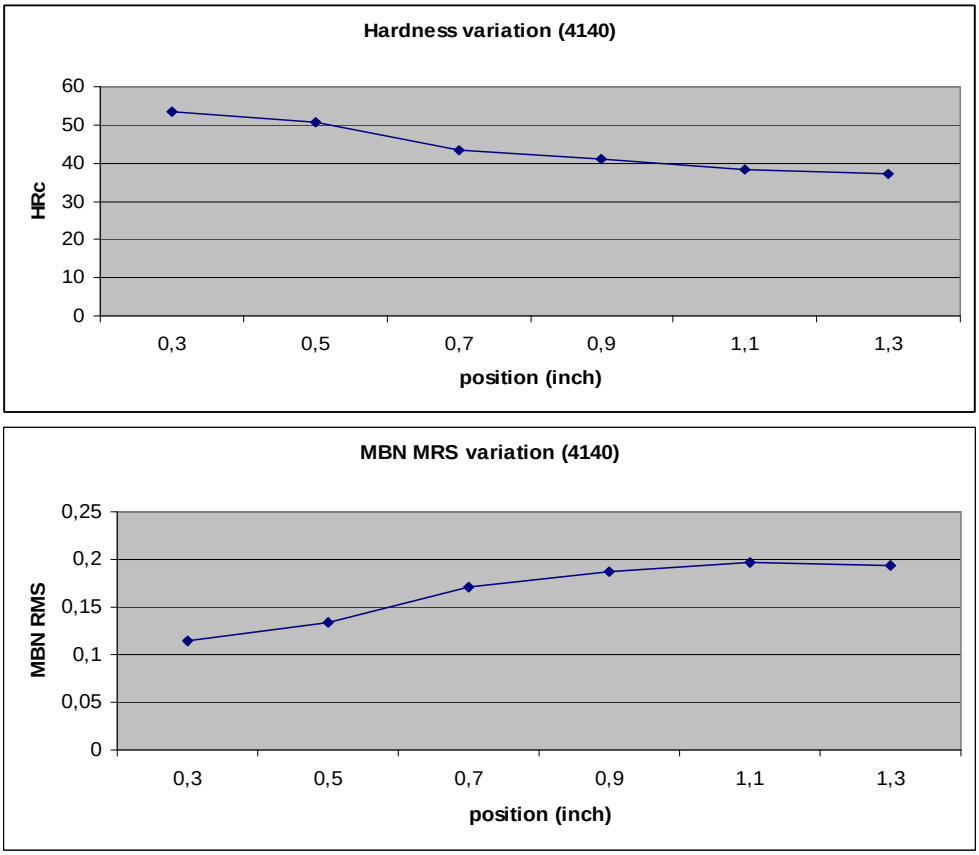

Figure 4. Hardness and MBN RMS variation throughout 4140 sample.

Therefore, a way to try solving this problem is to increase the dimension of the informational descriptor.

Figure 5 presents the average envelope of the MBN signal and the average envelope of the MBN spectrum. The MBN envelope gives more details of the MBN evolution with hardness. The amplitude and the area under curves increase with the decrease of hardness. But, similarly to what happens with the MBN RMS graphic, there is apparently not distinction between the signals associated with the last two hardness values. The envelopes of MBN spectra do not allow distinguishing among the last four values of MBN signals.

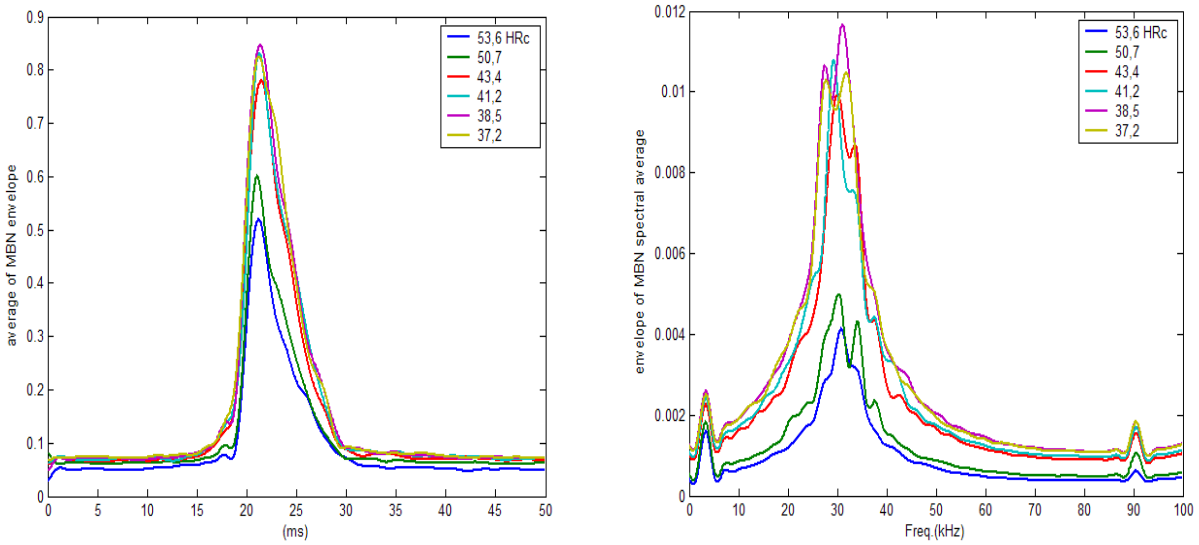

a) *b)*

Figure 5. a) Average envelope of MBN signals; b) Average envelope of MBN spectra

The TFRs and TSRs were calculated for all the hardness value cases, but, due to space limitation in this paper, only the results for the value of 53,6 HR are shown. As it is possible to see, the TFRs and TSRs are much richer in details than the scalar parameters and envelope representations.

It is important to observe that significant improvement in the quality of the TFRs representations can be reached by using averages of TFRs (or TSRs). This TFRs averaging process is done by calculating the TFR of each one of the 6 signals and then, averaging each point of these TFRs. The

same set of TFR parameters is used for each set of signals. Therefore, all TFRs images shown in Figure 6, Figure 7 and Figure 8 are averaged over 6 TFRs and are presented with amplitude (z-axes) normalized to one.

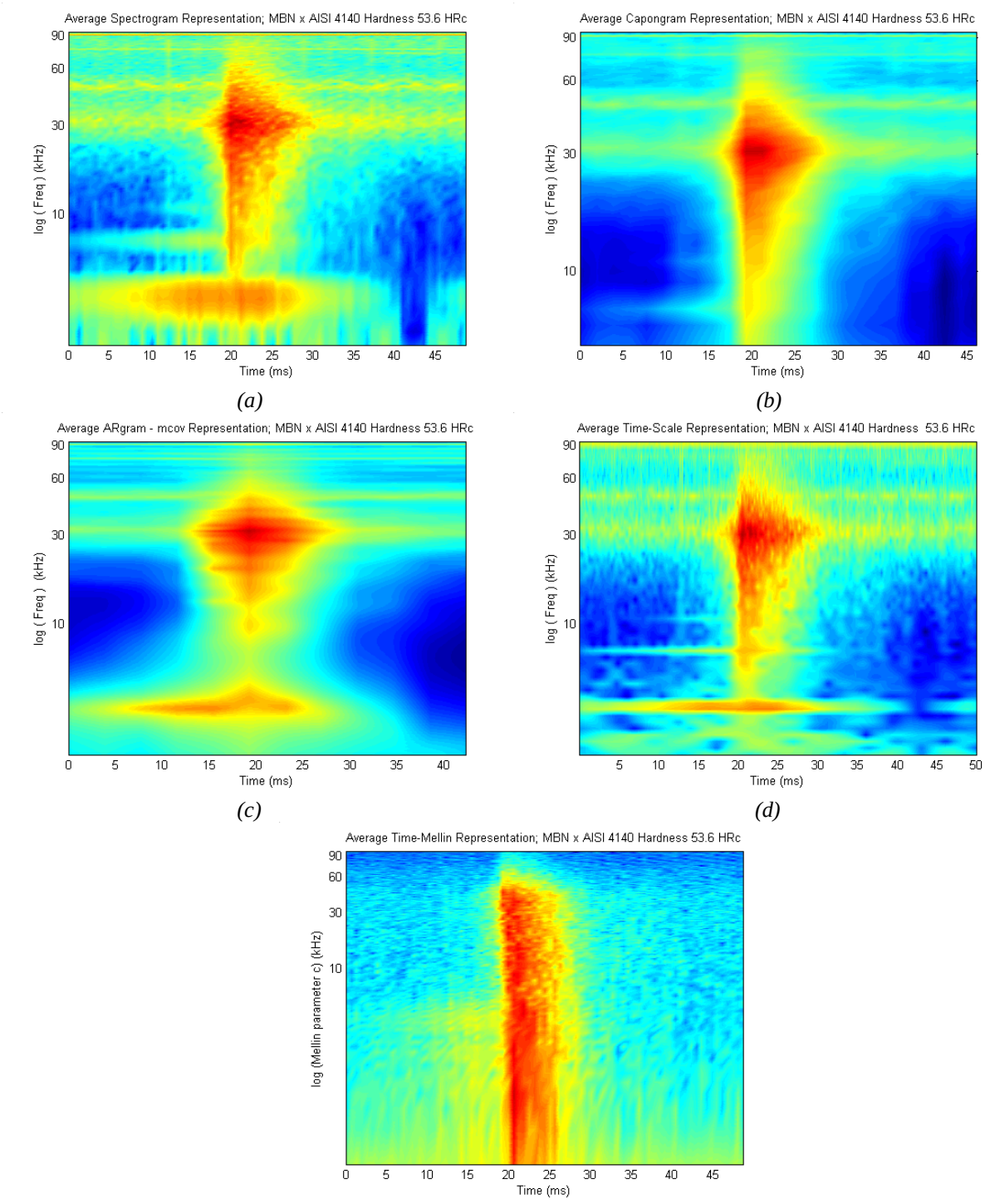

Figure 6. Average TFRs for 53.6 HRc signal with all frequency axes displayed in logarithm, TFR parameters reported in Table 1: a) Spectogram; b) Capongram; c) Argram; d) Scalogram; e) Mellingram

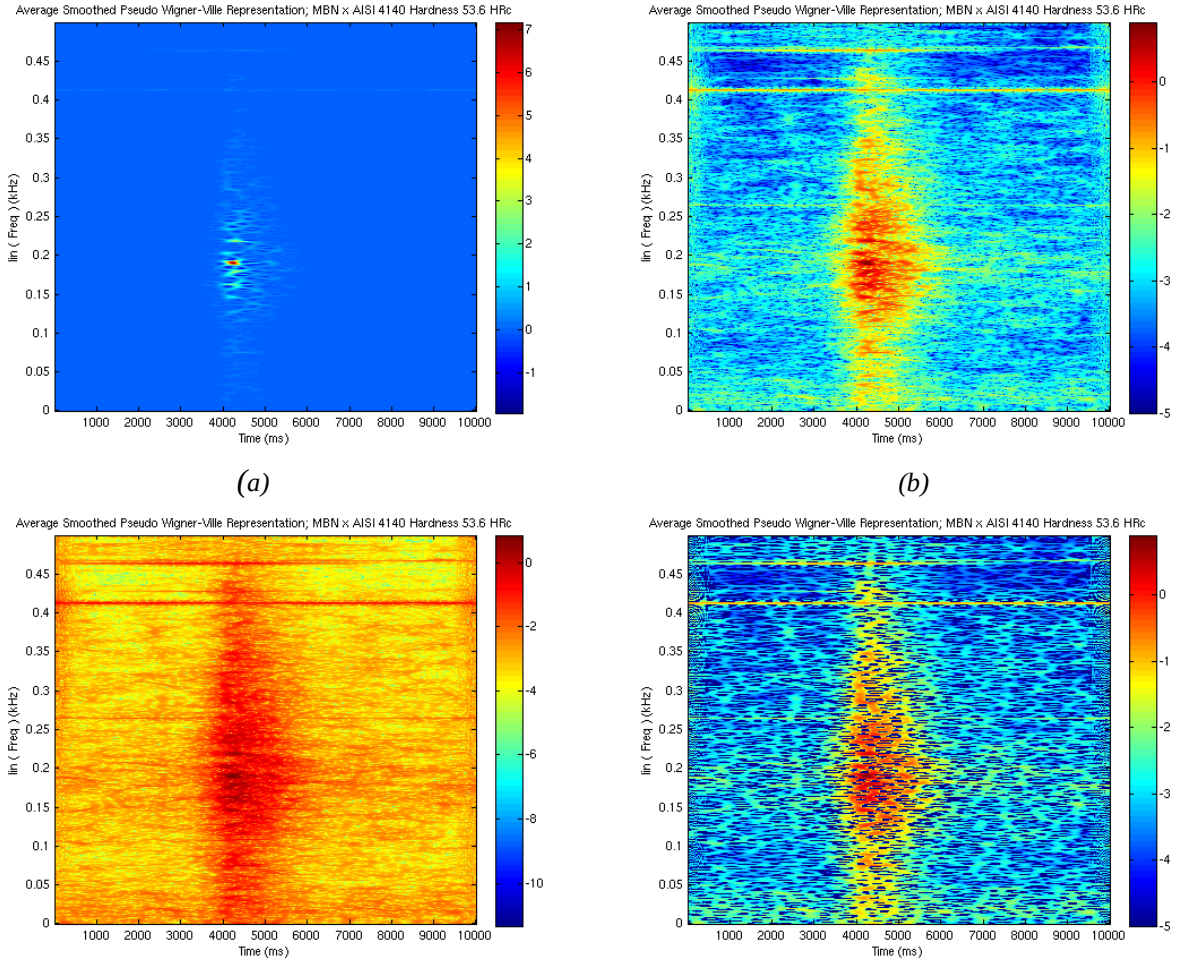

Figure 7. Average Smooth Pseudo Wigner-Ville's for 53.6 HRc signal obtained with a 16 GB RAM machine and with all frequency axes displayed in linear scale, parameters reported in table 1: a) linear scale of the TFR values; b) dB scale of the TFR absolute values between -5 and 0.9 dB; c) dB scale of all the TFR absolute values; d) dB scale of the TFR positive values only

By analysing the graphical representations of Figure 6, where all frequency axes are displayed in logarithm scale, it is interesting to notice that the Scalogram results are very similar to the TFRs ones. This means that there is no scale phenomenon (at least perceptible in this representation) in the MBN signals. Additionally, by analysing the Mellingram results, no scale structure could also be detected. Therefore, it seems that TFRs are enough to adequately describe the informational content of MBN signals.

Figure 7 shows the dilemma of a Wigner-Ville distribution which, independently of its high computational load, is a non-positive one. Different choices for the amplitude help for disjoining the

auto-terms for the cross-terms. Linear frequency components are well estimate but the MBN transitory structure is difficult to extract.

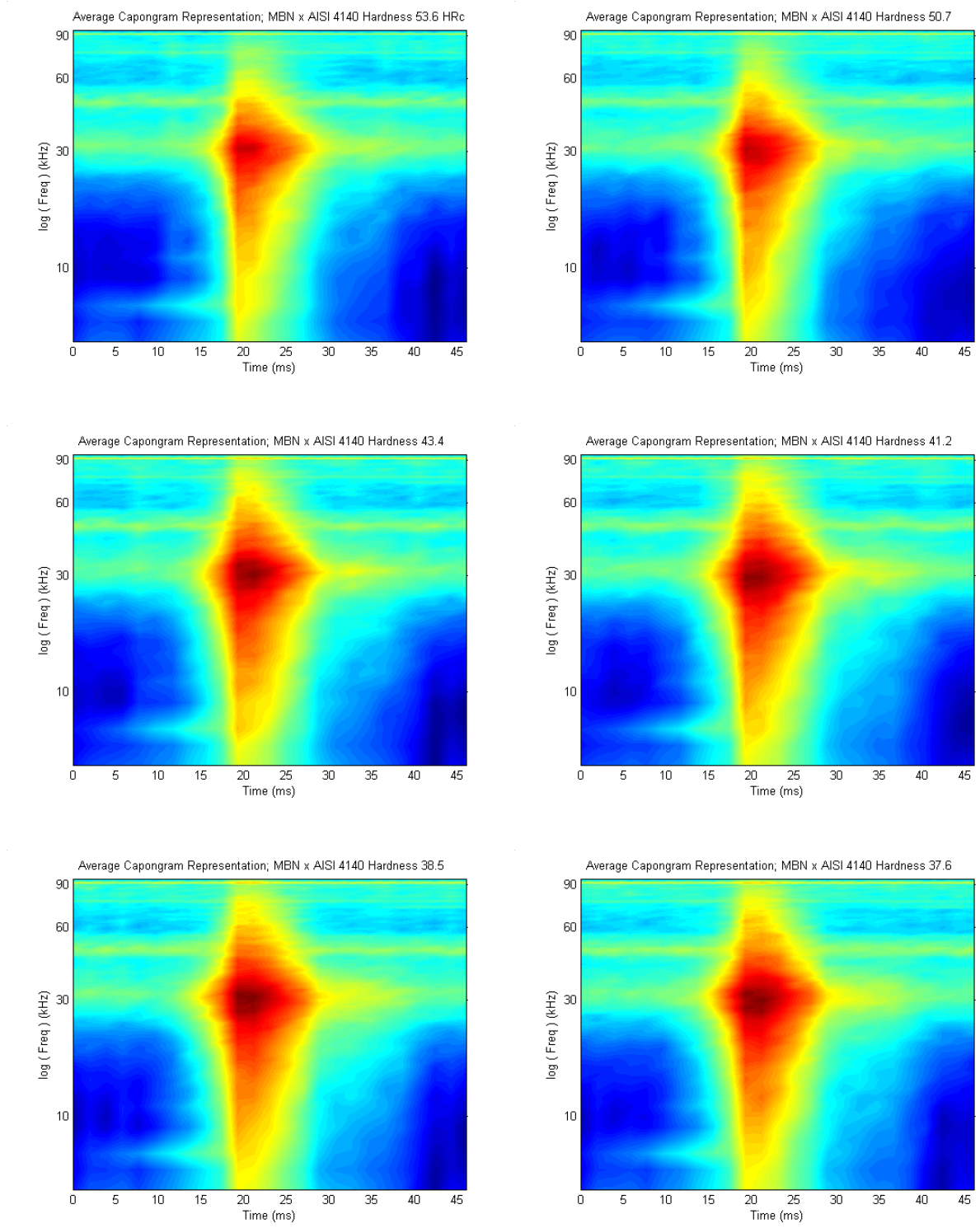

Figure 8. Average of Capongram's for different hardnesses in a AISI4140 steel, TFR parameters reported in Table 1

In Figure 8, the TFR corresponding to each one of the six hardness values are shown. The authors chose the Capongram method to illustrate the difference among them, since it is this method whose representations are the best among the TFRs and TSRs methods. Two main kinds of information can be taken out from Figure 6 and Figure 8. Stationary narrow-band frequencies are present all over the time duration of the signal (close to 30 kHz and 50 kHz). These frequencies cannot be related to MBN phenomenon (since the MBN is non-stationary). Therefore they may come from some external interferences of the measurement equipment.

The remaining information is on the non-stationarity of the MBN signals. All the information of the MBN envelope and of the MBN spectrum envelope is combined in the time-frequency domain in a synergetic way resulting in the richest panorama that can be seen from the MBN signals.

The differences among the MBN behaviours, for the six hardness values, are noticeable by the change in the general form of the time-frequency pattern, and in the pattern of the top of the 3-D surface.

7. Extraction of Characteristics from TFR

In order to highlight informational gain that the TFR can provide, to facilitate the interpretation and show some examples, among several others, of what can be done, two features of characteristic extraction are proposed: one vectorial and one scalar. With this two features, the dimension of the informational representation decreases by one. The first feature is the use of iso-level curves at a convenient TFR magnitude and the other is a cut of the TFR at a particular frequency or time value. All results of this section are obtained from the Capongrams.

Figure 9-a shows the frequency evolution of iso-level curves for each value of hardness at 40% of the highest TFR value. This threshold has been empirically chosen in order to find a characteristic time-frequency section validated by experts in the domain. At the end of this section, we propose an

automatic method in order to avoid such a choice. It is possible to note that, regarding to the frequency axes over 35 kHz, the curves seem to be more and more “lifted” with decreasing hardness values.

Figure 9-b shows a TFR cut of the Capongrams at 37 kHz. In this graphical representation, the expected correlation between hardness and MBN is clearly noticeable. The increase in the TFR values with the decrease of hardness is better represented than in the envelope case (Figure 5), particularly for the lowest values of hardness. Based on the results of Figure 9, Figure 10 shows the evolution of the normalized TFR amplitude with hardness.

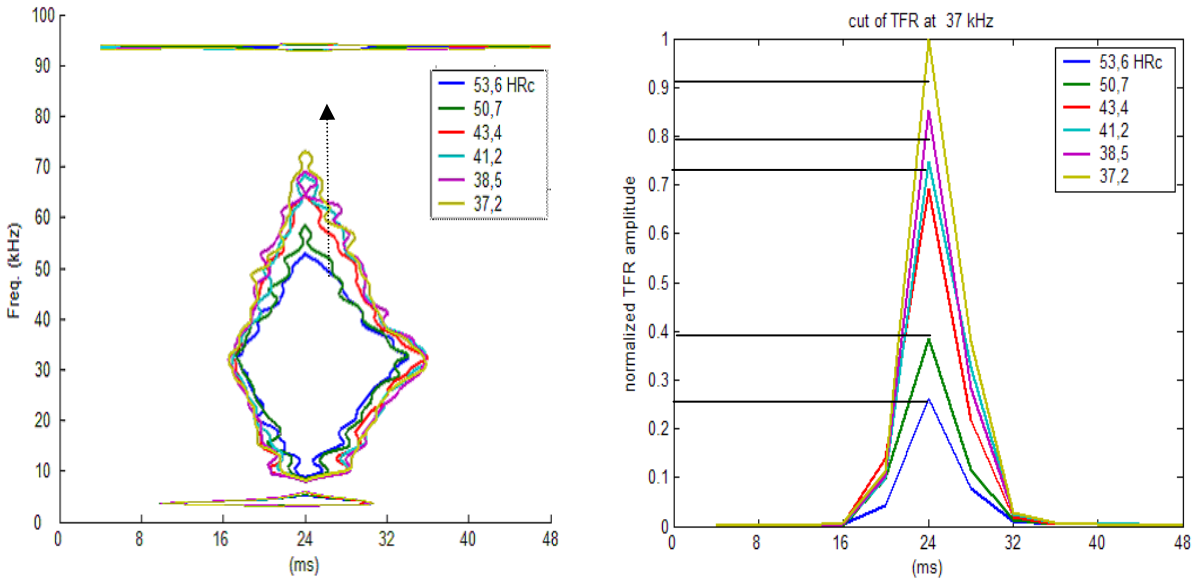

a) *b)*

Figure 9. a) Iso-level curves of the Capongrams of the different hardnesses in a AISI4140 steel at 40% of the highest value. b) Cut of the Capongram iso-level curves at the frequency of 37 kHz

Comparing Figure 10 with Figure 4 makes possible to see that the variation of the normalized TFR amplitude at 37 kHz with hardness is more significant than with the MBN RMS values. These results indicate that it is possible to find better information descriptors with TFR analysis than with the traditional 1D or 2D analysis.

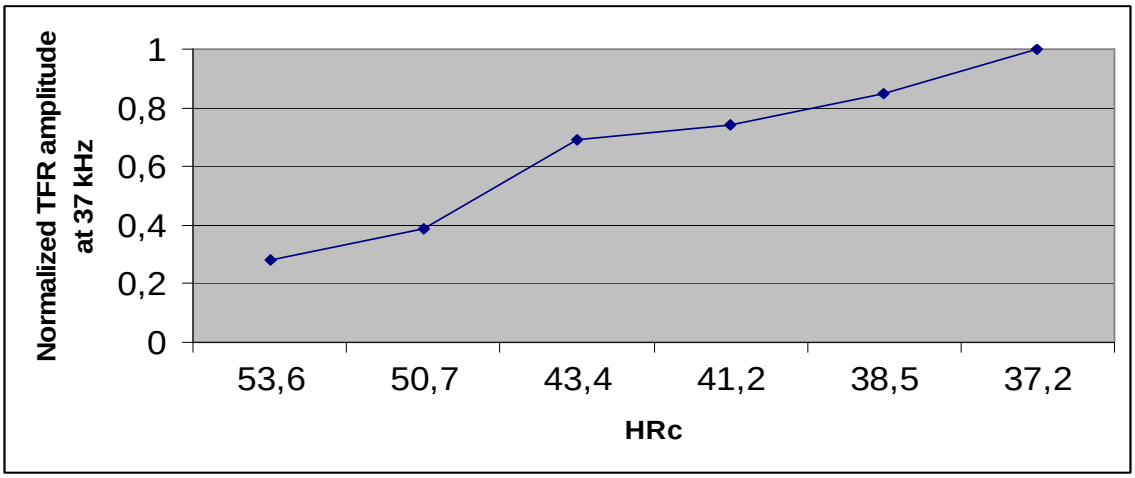

Figure 10. Variation of the normalized Capongram amplitude at 37 KHz, from Figure 8-b, with hardness.

This result brings now another question: Is it possible to obtain a method that automates this search? To that purpose, the authors have already published a method of automatic segmentation of some TFR such as the Short-Time Fourier transform and the spectrogram [17], [18]. This method has been adapted in order to be used from the Capongram, the TFR retained in this study.

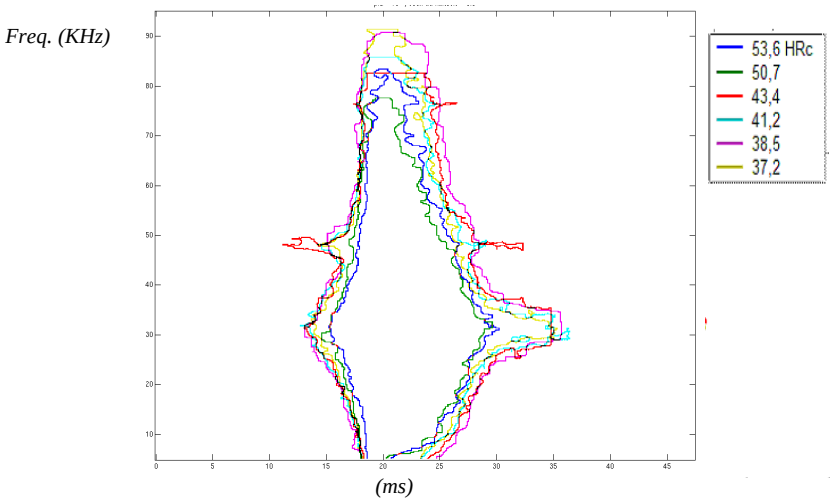

Figure 11. Automatic contour detection computed with Capongrams of the different hardnesses in a AISI4140 steel, Probability of false Alarm=10^{-2}, Kurtosis threshold=3.5.

Given that the theoretical basis of this method is out of the scope of this paper, only the method principle is described hereafter. Taking as signal model a nonstationary signal embedded in a white Gaussian noise, the probability density function of a time-frequency point is derived in order to determine the maximum likelihood estimator of the noise level. Then, an iterative algorithm allows the estimation of the noise level, from which a signal candidate set is determined according to a given probability of false alarm. Finally, an iterative region growing algorithm is applied to segment the different patterns of the representation. The segmentation stop is controlled by the Kurtosis of the remaining points, which should be low in order to characterize a Gaussian noise. For the MBN analysis, the adaptation has consisted to determine the degree of freedom of the chi-square law of a time-frequency point of a Capongram. In the case of the different hardnesses in a AISI4140 steel, Figure 11 shows the results of the automatic contour detection, which should be compared with Figure 9. This method gives the contour of the pattern bottom, from which a feature has to be defined for discriminating the different hardnesses.

These results indicate that the time-frequency domain opens a wide investigation field to define better information descriptors than with the traditional 1D or 2D analysis.

8. Conclusions

In this paper, a time-frequency strategy is proposed in order to use Magnetic Barkhausen Noise for characterizing the hardness level of a steel. This strategy consists of a time-frequency estimation followed by a self-working contour detection on the time-frequency representation. Although the TFR method can supply rich information on the Magnetic Barkhausen Noises, very few studies were actually undertaken with this magnetic phenomenon. In this paper, three Time-Frequency Representations and two Time-Scale Representations were used in order to analyse MBN measured in a steel sample with hardness variation, generated with a Jominy test. Having pointed out the vantages and disadvantages of each method, TFRs and TSRs of the same hardness value and TFR

for six different hardness values were presented. It was possible to observe that the TSRs did not show scales structures in the MBN signals. Results got from TFRs, and more particularly from the Capongram, yielded higher quality information of the MBN phenomenon than the traditional methods. The contours extracted were shown to be able to be relevant to the hardness level. Works are in progress on a wider MBN data set to validate the strategy proposed and to define the adequate time-frequency features in order to characterize not only the hardness but more generally the state of the material microstructure and the presence of deformations and mechanical stresses.

Acknowledgements

The authors wants to thanks to FAPESP (05/51100-9 and 06/04935-0) for the financial support and Eng. Freddy Franco for his add in the MBN measurements.

References

1. De Sena A.; La Trasformata di Mellin: teoria ed applicazioni all'analisi di segnali audio; Tesi de Laurea, Università degli Studi de Verona, 2003.
2. De Sena, A.; Rocchesso D.; A Fast Mellin and Scale Transform; EURASIP Journal on Advances in Signal Processing; Vol.2007, Article ID 89170, 9 pages, 2007.
3. Magalas, L. B.; Application of the wavelet transform in mechanical spectroscopy and in Barkhausen noise analysis; Journal of Alloys and Compounds, Vol.310, pp. 269–275, 2000.
4. Maass, P.; Teschke,G.; Willmann, W.; Günter Wollmann, G.; Detection and classification of Material Attributes - A Practical Application of Wavelet Analysis; IEEE Trans. On Signal Processing, Vol.48, pp. 2432 – 2438, August 2000.

5. Padovese, L.R.; Hybrid time-frequency methods for non-stationary mechanical signal analysis; Mechanical Systems and Signal Processing, Vol.18, pp.1047 - 1064, 2004.

6. Urbach, JS; Madison, RD; Markert, J; Interface Depinning, Self-Organized Criticality, and the Barkhausen effect; Physical Review Letters; Vol.75(2), pp. 276-279, 1995.

7. Pérez-Benitez, J. ; Capo-Sanchez, J. ; Anglada J. R. ; Padovese, L. R; A study of plastic deformation around a defect using the Magnetic Barkhausen Noise in ASTM 36 steel. NDT & E International, Vol.41, pp. 53-58, 2008.

8. Capo-Sanchez, J; Alberteris-Campos, M.; Padovese, L.R.; Magnetic Barkhausen measurements for evaluating the formation of Lüders bands in carbon steel, NDT & E Intern., Vol.40, pp. 520-524, 2007.

9. Altpeter, I.; Nondestructive evaluation of cementite content in steel and white cast iron using inductive Barkhausen noise. Journal of Nondestructive Evaluation.; Vol.15 (2); pp. 45-60, 1996.

10. Lachmann, C.; Nitschke-Pagel Th.; Wohlfahrt, H.; Characterization of residual stress Relaxation in Fatigue Loaded Welded Joints by X-Ray Diffraction and Barkhausen Noise Method. Materials Science Forum. Vol.347-349, pp.374-379, 2000.

11. Jeong,H.T.; Park, D.G.; Hong, J.H.; Ahn, Y.S.; Kim, G.M.; The effect of microstuctural changes on magnetic Barkhausen Noise in Mn-Mo-Ni pressure vessel steel. Journal of the Korean Physical Society. Vol.34, No.5, pp. 429-433, 1999.

12. Moorthy, V.; Shaw, B.A.; Evans, J.T.; Evaluation of tempering induced changes in the hardness profile of case-carburised EN steel using magnetic Barkhausen noise analysis. NDT&E International. Vol.36, pp 43-49, 2003.

13. Moorty, V.; Vaidyanathan, S.; Jayakumar,T.; Baldev RAJ.; Evaluation of post-weld heat treatment in 2,25Cr-1Mo steel tube to tube sheet welded joints using magnetic Barkhausen noise measurement. Materials Science and Technology. Vol.13, No.7, pp 614-617, 1997.

14. Cohen L.; Time Frequency Analysis: Theory and Applications; Prentice Hall Professional Technical Reference, December 1994.

15. Martin, N.; Minimum Variance, Spectral Analysis; Edited by F. CASTANIE; Traité IC2, Editeur HERMES, Chapter 7, pp 175-211, May 2006.

16. Martin, N.; An AR Spectral Analysis of Non Stationary Signals. Signal Processing, Vol.10, pp. 61-74, January 1986.

17. Millioz, F.; Huillery, J.; Martin, N.; Short Time Fourier Transform Probability Distribution for Time-Frequency Segmentation. IEEE International Conference on Acoustics, Speech, and Signal Processing, Proceedings of ICASSP 2006, pp. III-448-451, May 14-19 2006.

18. Millioz, F.; Martin, N.; Time-Frequency Segmentation for Engine Speed Monitoring, Special session on "Pattern Recognition in Acoustics and Vibration", Thirteen International Congress on Sound and Vibration, ICSV13, Vienna, Austria, July 2-6, 2006.

19. Mallat, S.; A Wavelet Tour of Signal Processing, Academic Press, 1999.

20. Zografos D.,Karagianni, K., Stouraitis, T.; VLSI architectures for the implementation of the Wigner distribution, IEEE International Symposium on Circuits and Systems, ISCAS 2002, Scottsdale, Arizona, USA, pp. IV-882- IV-885, vol.4, 2002.